# $N_2O$ Decomposition on MgO and Li/MgO Catalysts: A Quantum Chemical Study

**Xin Lu, Xin Xu,* Nanqin Wang, and Qianer Zhang**

*State Key Laboratory for Physical Chemistry of Solid Surfaces, Institute of Physical Chemistry, Department of Chemistry, Xiamen University, Xiamen 361005, PR China*

*Received: May 27, 1998; In Final Form: February 23, 1999*

Ab initio embedded cluster model calculations have been performed to study the decomposition of $N_2O$ on MgO and Li/MgO catalysts. The following has been found. (i) On MgO(001) terrace atomic oxygen is adsorbed on top of the $O_{5c}$ anions, while on corners or steps the preferable mode is for atomic oxygen to bridge over the low-coordinated $O_{XC}-Mg_{YC}$ ($X$, $Y = 3$, 4) ion pairs. The adsorption of atomic oxygen leads to the formation of a peroxide ion. (ii) $N_2O$ decomposition over a five-coordinate terrace anion would be possible, while the defective $O_{XC}-Mg_{YC}$ ($X$, $Y = 3$, 4) ion pairs are more active to decompose $N_2O$. The activity of the $O_{XC}-Mg_{YC}$ ($X$, $Y = 3$, 4) ion pairs toward $N_2O$ decomposition could be assigned in the order $O_{3C}-Mg_{3C} > O_{4C}-Mg_{3C} > O_{3C}-Mg_{4C} > O_{4C}-Mg_{4C}$. (iii) When the MgO catalyst is doped with Li, the so-called $[Li^+O^-]$ centers are found to be active for decomposing $N_2O$, and the decomposition of $N_2O$ on the active $[Li^+O^-]$ center leads to the formation of the superoxide anion. This accounts for the higher reactivity and selectivity of the Li/MgO catalyst.

## Introduction

The decomposition of $N_2O$ on metal oxides has been known for several decades.[1] Practically, $N_2O$ is always used as an oxidant in a lot of catalyzed oxidative processes, such as oxidative coupling of methane (OCM), oxidative dehydrogenation of alkanes, and so on.[2−8] $N_2O$ was suggested to provide adsorbed oxygen species on metal oxide catalysts and hence leads to specific oxidative selectivity.[2−8] For example, it was found that for the OCM reaction on Li/MgO catalysts, $N_2O$ works with higher $C_2$ selectivity and lower reaction temperature than $O_2$ does.[8] Therefore, the understanding of $N_2O$ decomposition on metal oxide catalysts and the properties of the relevant O adducts should be a good starting point for the understanding of the relevant catalytic processes.

Owing to its industrial importance, numerous experimental investigations have been carried out on the catalytic decomposition of $N_2O$ on metal oxides.[1−10] Early in 1970, Winter reported the results of a systematic experimental investigation regarding the catalytic activity of 40 metallic oxides for the decomposition of $N_2O$ to $N_2$ and $O_2$.[1] The mechanism supposed therein is, first, $N_2O$ adsorption on the catalysts, second, the adsorbed $N_2O$ decomposition to $N_2$ adspecies and atomic oxygen adspecies, and finally, the desorption of $N_2$ and $O_2$. For $N_2O$ decomposition on MgO, this mechanism was supported by the recent TPD experiments performed by Nakamura et al.,[10] despite that they detected no molecular $N_2O$ adsorption at reaction temperature (>523 K). The TPD experiments also revealed a rather low coverage of oxygen adspecies on the surface of the MgO catalyst after $N_2O$ decomposition, which suggested the sites' strongly binding O adspecies hould be the defective sites at kinks, steps, and corners.[10]

In contrast to a large number of experimental efforts on the reaction of $N_2O$ decomposition on metal oxides, little theoretical work has been done on such topic until recent years. The ab initio embedded cluster model calculations of Snis et al.[11] and DFT slab model calculations of Kontorovich et al.[12] revealed that on CaO, the decomposition of $N_2O$ occurs readily on five-coordinate surface anions (namely, $O_{5C}^{2-}$) with a linear $N_2-O-O_{5C}^{2-}$ transition state, leading to the formation of a peroxide-like surface species ($O_2^{2-}$). The existence of a peroxide-like surface species on CaO after $N_2O$ decomposition was evidenced by means of FT-IR spectroscopy.[6] It is natural for one to expect that a similar mechanism may hold true for the reaction on MgO. In fact, similar values of activation energies, i.e., ∼35 kcal/mol on MgO and ∼34 kcal/mol on CaO, were obtained experimentally by Winter.[1] However, recent TPD experiments[5,10] implied that the reaction on MgO would differ to some extent from that on CaO. Detailed theoretical studies regarding the decomposition of $N_2O$ on MgO catalyst are scarce. Some relevant papers published are those concerning atomic oxygen adsorption on the MgO(001) surface.[13−15] The ab initio embedded cluster calculations by Neygren and Petterson[13] and the DFT slab model calculations by Kantorovich and Gillan[14,15] both predicted that the favorable adsorption mode is for atomic oxygen to bind to a surface oxygen anion to form a peroxide ion ($O_2^{2-}$). While the former group predicted a very low binding energy of ∼10 kcal/mol for oxygen on top of an five-coordinate surface anion,[13] the latter found substantial binding energies of up to 46 kcal/mol for atomic oxygen adsorption at oxygen terrace sites and of over 58 kcal/mol at the surface irregularities.[14,15] Note that the energy cost to decompose $N_2O$ into $N_2$ and O in the gas phase is about 40 kcal/mol,[16] and a theoretical prediction of 50 kcal/mol from DFT/GGA calculations was given by Kantorovich and Gillan.[12] The results of the previous theoretical studies[13−15] indicate that decomposition of $N_2O$ on the low-coordinate anions, i.e., $O_{XC}^{2-}$ ($X = 3$, 4), at surface irregularities on MgO is thermodynamically favorable. No detailed information on how those low-coordinate anions, i.e., $O_{XC}^{2-}$ ($X = 3$, 4), are involved in the reaction of $N_2O$ decomposition is available. Whether the low-coordinate cations, i.e., $Mg_{YC}^{2+}$ ($Y = 3$, 4), are also involved in the activation of $N_2O$ remains a question.

* Corresponding author. E-mail: xinxu@xmu.edu.cn.

10.1021/jp982384+ CCC: $18.00 
Published on Web 04/09/1999

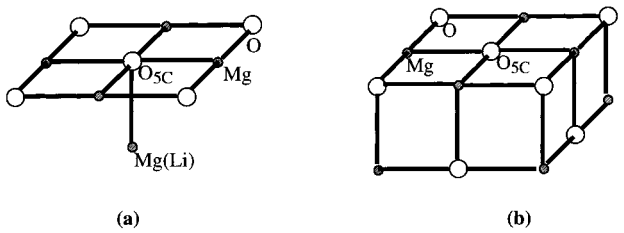


**Figure 1.** $(MgO)_5$ (a) and $(MgO)_9$ (b) local cluster models (O, circles; Mg, black dots).

Very recently, Snis et al.[17] performed both experiments and ab initio embedded cluster model calculations on the reaction of $N_2O$ decomposition on MgO(001) and CaO(001) surfaces. They, however, concluded that the $O_{5C}^{2-}$ sites are active for decomposing $N_2O$. In their CASPT2N calculations, the theoretical barrier heights are 33 and 22 kcal/mol for the reaction on MgO(001) and CaO(001), in accordance with their experimental activation energies of 36 and 26 kcal/mol, respectively. The reaction was predicted to be exothermic on CaO(001) ($\Delta E = -25$ kcal/mol) and to be endothermic on MgO(001) ($\Delta E = 3$ kcal/mol). It should be mentioned that their CASPT2N calculations underestimated the $N_2-O$ bonding energy for free $N_2O$ by 10 kcal/mol with respect to the experimental value of 40 kcal/mol,[16] which implies that the theoretical barrier heights, as well as the endothermicity, may be somewhat underestimated by their CASPT2N calculations. It seems that more experiments and theoretical work are required to verify the role of the five-coordinate anions ($O_{5C}^{2-}$) on MgO(001) surface.

Experimentally, it was found that Li-doping in MgO catalysts improves significantly the catalytic activity for $N_2O$ decomposition[7,10] but with a higher activation energy of ~46 kcal/mol[7] than that on pure MgO catalyst (~35 kcal/mol).[1] Li/MgO catalyst is also known as an effective OCM catalyst.[2,18] It was supposed that the Li-doping-induced $[Li^+O^-]$ centers facilitate the activation of methane, i.e., H-abstraction from $CH_4$.[2] This supposition has been supported by recent theoretical investigations.[19−22] However, the question of whether the $[Li^+O^-]$ center is active for decomposing $N_2O$ has not yet been of concern so far. We suppose, herein, that the $[Li^+O^-]$ center be active for decomposing $N_2O$, since atomic oxygen could be bound onto a surface $O^-$ anion, giving rise to an $O-O^-$ superoxy species with an energy gain possibly larger than the required value of 40 kcal/mol to break the $O-N_2$ bond. Note that the experimental value of O−O binding energy in $HO_2$ is 64 kcal/mol.[23]

In this paper, we report the results of comparative ab initio embedded cluster model calculations regarding the decomposition of $N_2O$ on solid MgO and Li-doped solid MgO. We will address (i) which sites are active for decomposing $N_2O$ on MgO and Li/MgO catalysts, (ii) the transition states and the corresponding barrier heights of $N_2O$ decomposition, and (iii) how Li-doping promotes the reactivity of the MgO catalyst toward $N_2O$ decomposition.

**Computational Details.** MgO has the rock-salt structure.[24] The five-coodinate anion site on the MgO(001) surface was simulated by a neutral, stoichiometric $(MgO)_5$ cluster (Figure 1a) embedded within a (11 × 11 × 6−10) MgO microcrystal, with a local symmetry of $C_{4v}$. A larger cluster model, the $(MgO)_9$ cluster (Figure 1b) embedded within a (11 × 11 × 6−18) MgO microcrystal, was employed to check the size effect of cluster models. The clusters $(MgO)_n$ ($n = 4, 6, 8$), employed to model the low-coordinate (three- or four-coordinate) surface sites, were shown in Figures 2 and 3. These clusters were placed on the surface or placed at the corner or edge of a (10 × 10 × 10) microcrystal, respectively, as depicted in Figure 2. As such,

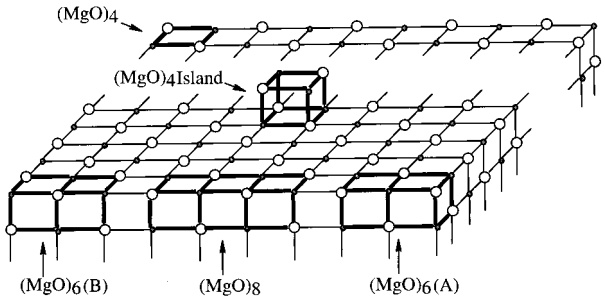


**Figure 2.** Brief view of the MgO (10 × 10 × 10) microcrystal and the embedded cluster models (○, circles; Mg, black dots).

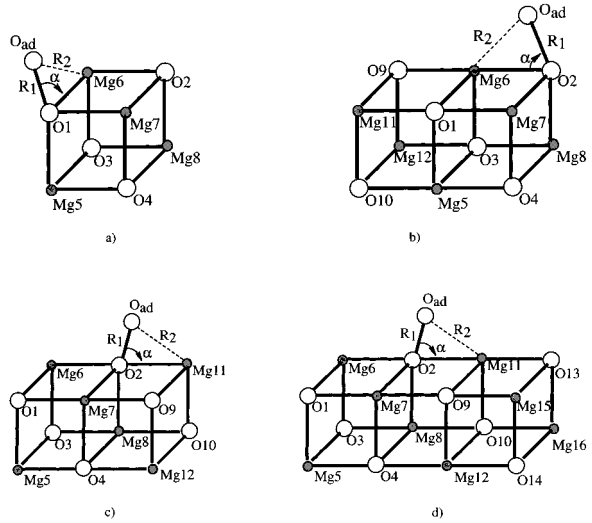


**Figure 3.** $(MgO)_n$ clusters: (a) $(MgO)_4$; (b) $(MgO)_6$(A); (c) $(MgO)_6$-(B); (d) $(MgO)_8$. O adatoms are bound to $O_{3C}-Mg_{3C}$, $O_{4C}-Mg_{3C}$, $O_{3C}-Mg_{4C}$, $O_{4C}-Mg_{4C}$ pair sites, respectively (○, circle; Mg, black circle).

we have five embedded cluster models. They are the $(MgO)_4$ island at the center of the (001) surface with both $O_{3C}$ and $Mg_{3C}$ exposed, $(MgO)_4$ at a corner site with an $O_{3C}$ anion and a $Mg_{4C}$ cation exposed, $(MgO)_6$(A) at a corner site with an $O_{3C}$ anion and a $Mg_{4C}$ cation exposed, $(MgO)_6$(B) at a corner site with an $O_{4C}$ anion and a $Mg_{3C}$ cation exposed, and $(MgO)_8$ at a step site with an $O_{4C}$ anion and a $Mg_{4C}$ cation exposed.

The $[Li^+O^-]$ center on the Li/MgO surface was modeled by a LiO dimer embedded within a (11 × 11 × 6−2) MgO microcrystal with the $O^-$ anion exposed on the MgO(001) surface. It was assumed that Li was simply to replace the lattice Mg cation in the second layer of the MgO(001) surface. A larger cluster model, namely, $LiMg_4O_5$ (see also Figure 1a), has also been employed to model such a $[Li^+O^-]$ center. The embedded $LiMg_4O_5$ cluster was obtained by simply replacing the second-layer Mg atom of the embedded $(MgO)_5$ cluster model with a Li atom (Figure 1a).

For all these embedded cluster models described above, the MgO or Li/MgO surface was simulated explicitly by an atomistic cluster of a given size with the rest of the anions and cations of the microcrystal being approximated by point charges (PCs). The values of the PCs employed here were determined self-consistently to be ±1.75.[25] The charge-consistence technique has also been successfully employed in our previous papers regarding CO/NiO[26] and $H_2$/ZnO[27] chemisorption systems. Similar effective Madelung charges of ±1.8 have been recommended by Rösch et al. on the basis of their DFT slab model calculations of the MgO(001) surface.[28] Since the positive PCs would significantly distort the electron density of the anions on the cluster boundaries, the nearest positive PCs were

**TABLE 1: B3LYP/MP2 Bond Lengths of $N_2$, $O_2$, NO, and $N_2O$ and the Corresponding Dissociation Energies[a]**

| | $R_e$(N−N) (Å) | $R_e$(N−O) (Å) | $R_e$(O−O) (Å) | $D_e$ (kcal/mol) |
|---|---|---|---|---|
| $N_2$ | 1.105/1.131 (1.098) | | | 222.3/215.6 (228) |
| $O_2$ | | | 1.215/1.246 (1.208) | 120.7/117.3 (120) |
| NO | | 1.158/1.143 (1.151) | | 150.7/139.6 (150) |
| $N_2O$ | 1.133/1.172 (1.126) | 1.195/1.196 (1.188) | | 44.5/42.2 (40)[b] |

[a] Data in parentheses are the experimental values.[16] [b] The dissociation energy corresponds to the gas-phase reaction $N_2O \rightarrow N_2 + O(^3P)$.

augmented with Ne core potentials of Mg[29] to include the effect of Pauli repulsion.

We have used the hybrid density functional B3LYP[30,31] method, as implemented in the Gaussian-94 suite of programs.[32] For most cases considered, the basis sets employed are standard, i.e, 6-31+G* basis sets[32] for O and N atoms and 6-31G* basis sets[32] for Mg and Li atoms. The natural bond orbital (NBO) method[33] was used for wave function analysis in some cases. For comparison, the reactions on the embedded $(MgO)_5$, $(MgO)_9$, LiO, and $LiMg_4O_5$ cluster models were also investigated by means of the MP2 method (the second-order Møller−Plesset perturbation theory).[34,35] In the MP2 calculations with the embedded $(MgO)_5$, $(MgO)_9$, and $LiMg_4O_5$ cluster models, only the O and M atoms in the central OM (M = Mg, Li) dimer were described with the standard 6-31G* and 6-31+G* basis sets,[32] while the rest of the Mg atoms and O atoms were described with CEP-4G basis sets[29,32] and CEP-31G basis sets,[29,32] respectively.

Table 1 presents the results of our B3LYP or MP2 calculations for some relevant molecules and reactions in the gas phase, which are in agreement with the experimental values.

## Results and Discussions

**1. Atomic O adsorption on an $O_{5C}^{2-}$ Terrrace Site.** We first considered atomic oxygen adsorption on an $O_{5C}^{2-}$ terrace site. By use of a minimal cluster model, i.e., an embedded $O^{2-}$ anion, the previous MCPF (modified coupled pair functional method) calculation performed by Nygren and Pettersson[13] predicted an adsorption energy of 10.4 kcal/mol for oxygen adsorption at the five-coordinate anion site on the MgO(001) surface. Previous DFT slab model calculations by Kantorovich et al.,[14,15] however, gave a larger value of 46 kcal/mol. Our B3LYP calculation with the embedded $(MgO)_5$ cluster model gave a binding energy of 25.3 kcal/mol, which lies between the previous theoretical values. Our B3LYP optimized $O_{ad}-O_{5C}$ bond length is 1.521 Å, slightly shorter than the previous MCPF and DFT results (∼1.55 Å).[13−15] Our MP2 calculation gave comparable results with those of B3LYP. The optimal $O_{ad}-O_{5C}$ bond length is 1.502 Å, and the calculated binding energy is 19.6 kcal/mol in MP2.

**2. Atomic O Adsorptions on Low-Coordinate $O_{XC}$ and $Mg_{YC}$ ($X, Y = 3, 4$) Sites at Corners and Steps**. We then report the calculation results of atomic O adsorptions on low-coordinate $O_{XC}$ and $Mg_{YC}$ (X,Y = 3, 4) sites at corners and steps with bare $(MgO)_n$ ($n = 4, 6, 8$) cluster models. The purpose of these calculations is twofold, i.e. to investigate the size dependence of the cluster models and to evaluate the influence of the long-range crystal potential.

B3LYP-optimized geometries and the corresponding binding energies for O adsorptions on bare $(MgO)_n$ ($n = 4, 6, 8$) clusters are given in Figure 3 and Table 2. We found that O absorbs onto the $O_{XC}$ ($X = 3, 4$) sites preferably with the $O_{ad}-O_{XC}$ bond tilting toward a neighboring $Mg_{YC}$ atom. This kind of configuration may be naively interpreted as a result of the electrostatic interaction between the negatively charged O adatom and the nearby $Mg_{YC}$ cation. However, the $O_{ad}-Mg_{YC}$ ($Y = 3, 4$) distances, ranging from 1.966 to 1.923 Å, are shorter than the distance of 2.104 Å[24] for Mg−O ion pairs in bulk MgO, implying that substantial covalent interaction may exist between $O_{ad}$ and $Mg_{YC}$. This covalent interaction is verified by means of NBO analysis and will be discussed later in this section.

**TABLE 2: B3LYP-Optimized Geometries for Atomic O Adsorption on Bare $(MgO)_n$ ($n = 4, 6, 8$) and the Corresponding Binding Energies[a]**

| cluster and symmetry | pair site | $R_{O-O}$ (Å) | $R_{Mg-O}$ (Å) | α | β | $D_e$ (kcal/mol) |
|---|---|---|---|---|---|---|
| $(MgO)_4$, $C_s$ | $O_{3C}-Mg_{3C}$ | 1.513 | 1.928 | 61.9 | 135.0 | 60.6 |
| $(MgO)_6$, $C_1$ | $O_{3C}-Mg_{3C}$ | 1.515 | 1.923 | 61.7 | 135.0 | 60.1 |
| $(MgO)_8$, $C_1$ | $O_{3C}-Mg_{3C}$ | 1.515 | 1.923 | 61.8 | 134.9 | 59.4 |
| $(MgO)_6$, $C_s$ | $O_{4C}-Mg_{3C}$ | 1.534 | 1.935 | 62.0 | 135.0 | 56.0 |
| $(MgO)_8$, $C_s$ | $O_{4C}-Mg_{3C}$ | 1.529 | 1.934 | 62.0 | 135.0 | 54.0 |
| $(MgO)_6$, $C_s$ | $O_{3C}-Mg_{4C}$ | 1.502 | 1.953 | 63.0 | 135.0 | 49.8 |
| $(MgO)_8$, $C_s$ | $O_{3C}-Mg_{4C}$ | 1.502 | 1.953 | 63.0 | 135.0 | 50.2 |
| $(MgO)_8$, $C_s$ | $O_{4C}-Mg_{4C}$ | 1.526 | 1.966 | 63.2 | 135.0 | 45.4 |

[a] $D_e = E[(MgO)_n] + E[O(^3P)] - E[(MgO)_n-O]$.

As suggested by the previous DFT slab model calculations,[14,15] the most preferable geometry for atomic oxygen adsorption at the terrace sites and at the irregularities on MgO is that the $O_{ad}-O_{XC}$ bond tilts toward a neighboring surface anion. For the sake of clarification, we called the adsorption mode obtained in the present work a "bridge mode" and the adsorption mode obtained in the previous DFT slab model calculations a "tilted mode". We should point out that the bridge mode presently concerned was not examined in the previous DFT slab model calculations.[14,15] For comparison, we performed B3LYP calculations for O adsorption on the $O_{3C}$ site of $(MgO)_4$ with the tilted mode. In this mode, the optimized $O_{ad}-O_{3C}$ bond length is 1.516 Å, and the $O_{ad}-O_{3C}$ bond tilts to the neighboring $O_{3C}$ atom with a $\angle O_{ad}-O1-O2$ bond angle of 65.9° (see Figure 3a for the positions of O1 and O2), in accordance with the DFT slab model calculations.[14,15] However, the calculated binding energy for the tilted mode is 47.9 kcal/mol, i.e., by ∼13.0 kcal/mol unstable with respect to the bridge mode. Further calculations with larger cluster models $(MgO)_6$ and $(MgO)_8$ gave the same results. For example, for O adsorption at the $O_{4C}$ site of the $(MgO)_8$ cluster, the tilted mode (toward a neighboring $O_{4C}$) is found to be unstable by ∼7.0 kcal/mol in energy with respect to the bridge mode (over the $O_{4C}-Mg_{4C}$ pair site). This finding suggests that the active sites responsible for atomic oxygen adsorption at the corners and steps on the MgO(001) surface are better referred to as $O_{XC}-Mg_{YC}$ ($X, Y = 3, 4$) pair sites rather than single low-coordinate anion sites, which was suggested by the previous DFT slab model calculations.[14,15] This has been further verified by the subsequent embedded cluster model calculations.

From an inspection of the calculated binding energies and geometry parameters listed in Table 2, we make the following remarks.

(i) For the adsorptions at the $O_{3C}-Mg_{3C}$ pair sites, the calculated binding energy and the geometry parameters with $(MgO)_n$ ($n = 4,6,8$) models show negligible dependence on the cluster size. For all these three clusters, the binding energies

**TABLE 3: B3LYP-Optimized Geometries for Atomic O Adsorption on Embedded $(MgO)_n$ ($n$ = 4, 6, 8) and the Corresponding Binding Energies[a]**

| Cluster and symmetry | embedded site | pair site | $R(O_{ad}-O_{LC})$ (Å) | α | $\beta$ | $D_e$ (kcal/mol) | $\omega_e$ ($cm^{-1}$) |
|---|---|---|---|---|---|---|---|
| $(MgO)_4$, $C_s$ | corner | $O_{3C}-Mg_{4C}$ | 1.516 | 62.7 | 135.0 | 56.7 | |
| | | $O_{3C}-O_{5C}$[b] | 1.516 | 67.5 | | 47.0 | |
| $(MgO)_4$, $C_1$ | island | $O_{3C}-Mg_{3C}$ | 1.503 | 61.1 | 139. | 72.5 | 819 |
| $(MgO)_6$(A), $C_s$ | corner | $O_{3C}-Mg_{4C}$ | 1.512 | 63.0 | 135.0 | 53.9 | 850 |
| | | $O_{3C}-O_{5C}$[b] | 1.516 | 65.7 | | 46.1 | |
| $(MgO)_6$(B), $C_s$ | corner | $O_{4C}-Mg_{3C}$ | 1.512 | 62.0 | 135.0 | 58.3 | 827 |
| | | $O_{4C}-O_{4C}$[b] | 1.522 | 67.6 | | 42.5 | |
| $(MgO)_8$, $C_s$ | step | $O_{4C}-Mg_{4C}$ | 1.526 | 63.2 | 135.0 | 49.8 | 857 |
| | | $O_{4C}-O_{5C}$[b] | 1.520 | 67.5 | | 40.8 | |

[a] $D_e = E[(MgO)_n] + E[O(^3P)] - E[(MgO)_n-O]$. [b] Tilted mode adsorption, $\alpha = \angle O_{ad}-O_{XC}-O_{YC}$.

are found to be around 60 kcal/mol, the $O_{ad}-O_{3C}$ bond lengths around 1.51 Å, the $\angle O_{ad}-O_{3C}-Mg_{3C}$ angles around 62.8°, and the $O_{ad}-Mg_{3C}$ distances around 1.92 Å. The same trend holds true for the adsorptions at the $O_{3C}-Mg_{4C}$ pair sites and the $O_{4C}-Mg_{3C}$ pair sites on $(MgO)_6$ and $(MgO)_8$. This feature suggests that these three cluster models give a convergent description of the adsorption properties.

(ii) On the other hand, the computed properties show a clear site dependence. The calculated binding energies range from ~60 kcal/mol for the adsorption at $O_{3C}-Mg_{3C}$ to ~45 kcal/mol for the adsorption at $O_{4C}-Mg_{4C}$. As such, the activity of these pair sites to oxygen adsorption can be assigned in the order $O_{3C}-Mg_{3C} > O_{4C}-Mg_{3C} > O_{3C}-Mg_{4C} > O_{4C}-Mg_{4C}$.

(iii) It is interesting to compare the relative activity between $O_{4C}-Mg_{3C}$ and $O_{3C}-Mg_{4C}$. Generally speaking, $O_{3C}$ should be more active than $O_{4C}$, while $Mg_{3C}$ is more active than $Mg_{4C}$. Indeed, the optimized $O_{ad}-O_{3C}$ bond length (1.50 Å) for $O_{ad}$ bridging over the $O_{3C}-Mg_{4C}$ pair is shorter than the optimized $O_{ad}-O_{4C}$ bond length (1.53 Å) for $O_{ad}$ bridging over the $O_{4C}-Mg_{3C}$ pair, while the optimized $O_{ad}-Mg_{4C}$ distance (1.95 Å) is longer than the $O_{ad}-Mg_{3C}$ distance (1.93 Å). The binding energy on the $O_{4C}-Mg_{3C}$ pair is ~5 kcal/mol higher than that on the $O_{3C}-Mg_{4C}$ pair, which reflects the important contribution from the nearby cations.

NBO analysis has been performed to assess the nature of the bond between $O_{ad}$ and the low-coordinate sites. The NBO charges on $O_{ad}$ and $O_{XC}$ are around 0.8 and 1.0 au, respectively, which clearly demonstrates that the dioxygen surface species, $(O_{ad}-O_{XC})^{1.8-}$, are peroxide-like. More interestingly, we have found a substantial charge transfer from the lone pair of the $O_{ad}$ to the empty orbital at the $Mg_{YC}$ site. This is in line with the fact that the $O_{ad}-Mg_{YC}$ bond length is shorter than the Mg−O distance in the bulk solid. The strengths of the orbital interactions can be estimated by perturbative analysis of the Fock matix in the NBO basis. The energy contribution owing to this interaction varies from 23 to 27 kcal/mol according to the type of adsorption site. The significance of such a substantial dative bonding between the adsorbed oxygen atoms and the $Mg_{YC}$ ($Y$ = 3, 4) is that it may facilitate O-exchange between the O adatoms and the related lattice anions at elevated temperature.

With the embedded cluster models, the B3LYP calculations indicate that the bridge mode outweighs the tilted mode and that the adsorption properties are more site-dependent than size-dependent. The results of such comparative calculations are given in Table 3.

For the embedded $(MgO)_4$ cluster at the corner site, we have studied the O adsorption onto the $O_{3C}$ anion in a bridge mode or in a tilted mode. In the tilted mode, the optimized $O_{ad}-O_{3C}$ bond length is 1.516 Å and the $\angle O_{ad}-O_{3C}-O_{5C}$ angle 67.5°; while in the bridge mode, the optimized $O_{ad}-O_{3C}$ bond length is 1.516 Å and the $\angle O_{ad}-O_{3C}-Mg_{4C}$ angle is 62.7°. Energetically, the bridge mode is superior by about 10 kcal/mol to the tilted mode. For the larger cluster, i.e., the embedded $(MgO)_6$(A) cluster, in which the step-sitting $Mg_{4C}$ atom is coordinated perfectly by four real O atoms, the results obtained are very similar to those from the corner site $(MgO)_4$. The binding energy for O adsorption on the $O_{3C}-Mg_{4C}$ ion pair obtained with the embedded $(MgO)_6$(A) is only 3 kcal/mol lower than that obtained with the embedded $(MgO)_4$ cluster. With the embedded $(MgO)_6$(B) cluster and the embedded $(MgO)_8$ cluster, the preferable mode for atomic oxygen adsorption at the $O_{4C}$ sites is found to bridge over the $O_{4C}-Mg_{3C}$ pair and the $O_{4C}-Mg_{4C}$ pair, respectively. For example, for oxygen adsorption at the step-sitting $O_{4C}$ site on the embedded $(MgO)_8$ cluster, the bridge mode (over the step-sitting $O_{4C}-Mg_{4C}$ ion pair) is calculated to be ~9 kcal/mol more stable than the tilted mode (toward a neighboring $O_{4C}$ anion) (cf. Table 3). As such, we advocate that the preferable adsorption mode for atomic oxygen adsorbed at a low-coordinate $O_{XC}$ ($X$ = 3, 4) anion site is for the $O_{ad}-O_{XC}$ bond to tilt to a neighboring $Mg_{YC}$ cation rather than to tilt to a neighboring anion.

From Table 3, we note that the inclusion of long-range crystal potential has not altered considerably the optimized geometries with respect to those obtained by using bared cluster models. The binding energies obtained by using embedded cluster models are about 4 kcal/mol larger than those obtained with bared cluster models, except for the case of O adsorption on the $O_{3C}-Mg_{3C}$ ion pair, for which the inclusion of the long-range crystal potential of the bulk solid induces an increase of ~12 kcal/mol in the predicted binding energy. The activity of the $O_{XC}-Mg_{YC}$ ion pairs toward atomic O adsorption can be assigned in the same order as that obtained by using bared cluster models, i.e. $O_{3C}-Mg_{3C} > O_{4C}-Mg_{3C} > O_{3C}-Mg_{4C} > O_{4C}-Mg_{4C}$.

The optimized $O_{ad}-O_{XC}$ bond lengths range from 1.50 to 1.53 Å, shorter than the O−O distance of 1.569 Å in the free $O_2^{2-}$ ion obtained by means of B3LYP calculations. The O−O bond lengths of $O_2^{2-}$ ions in peroxide salts were found to be in the range from 1.49 Å (e.g., in $BaO_2$) to 1.54 Å (e.g., in $Rb_2O_2$),[36] in agreement with our calculated values. We have calculated the $O_{ad}-O_{XC}$ stretching frequency of the so-formed peroxide ions. The vibrational frequencies, $\omega_e$(OO), were determined by a 4th-degree polynomial fit to five points around the minimum of the corresponding potential energy curves. The calculated $\omega_e$(OO)'s are in the range 819−857 $cm^{-1}$ (cf. Table 3) with respect to the adsorption sites concerned. So far, there is no IR spectra reported for the O/MgO system. Studies of metal−dioxygen complexes[37] showed that the peroxide-like complexes have IR bands in the range 800−932 $cm^{-1}$. On oxygen-preadsorbed Ba/MgO catalysts, an in situ Raman study[38] indicated three bands at 842, 829, and 821 $cm^{-1}$, which were

**TABLE 4: Transition States, Barrier Heights,[a] and Reaction Heats[b] of $N_2O$ Decomposition on Five-Coordinate Anionic Center at MgO(001) and on the [$Li^+O^-$] Center at Li/MgO(001) Surfaces[c]**

| embedded cluster | method | $R_{O-O}$ (Å) | $R_{N-O}$ (Å) | $E^{TS}$ (kcal/mol) | $\Delta E$ (kcal/mol) |
|---|---|---|---|---|---|
| $(MgO)_5$ | B3LYP | 1.90 | 1.65 | 42.0 | 19.2 |
| | MP2 | 1.86 | 1.61 | 58.4 | 22.6 |
| $(MgO)_9$ | B3LYP | 1.96 | 1.61 | 36.0 | 4.7 |
| | MP2 | 1.88 | 1.57 | 53.3 | 8.6 |
| LiO | B3LYP | 1.80 | 1.57 | 47.4 | −26.9 |
| | MP2 | 1.82 | 1.56 | 60.0 | −17.1 |
| $LiMg_4O_5$ | B3LYP | 1.95 | 1.58 | 35.6 | −8.5 |
| | MP2 | 1.80 | 1.65 | 48.5 | −7.7 |

[a] $E^{TS} = E[(\text{surface cluster})-O-N_2] - E(\text{surface cluster}) - E(N_2O)$. [b] $\Delta E = E[(MgO)_n-O] + E(N_2) - E[(MgO)_n] - E(N_2O)$. [c] The N−N distance was fixed to 1.126 Å.

ascribed to peroxide ions. On CaO catalysts after $N_2O$ decomposition, Nakamura and co-workers detected the existence of peroxy ions with an IR band at ~880 $cm^{-1}$, by means of FTIR spectroscopy.[6] Our calculated $\omega_e$(OO)'s for the peroxy ions at the defective sites on the MgO(001) surface are in good agreement with these experimental values.

**3. $N_2O$ Decomposition over Terrace Site on MgO.** Previous ab initio embedded cluster model calculations[11] have shown that molecular adsorption of $N_2O$ on CaO could be regarded as physisorption. We believe that the same is true for $N_2O$ adsorption on MgO. In fact, the TPD experiment showed that molecular adsorption of $N_2O$ on the MgO solid surface is very unlikely at reaction temperature.[10] Therefore, we did not consider $N_2O$ molecular adsorption on MgO.

The experimental value of the energy cost for $N_2O$ decomposition toward $N_2$(g) and O($^3$P) in the gas phase is about 40 kcal/mol,[16] while the B3LYP calculation in the present work gives a value of 44.5 kcal/mol (cf. Table 1). As predicted in the previous sections, the binding energies for atomic O adsorption onto the $O_{XC}-Mg_{YC}$ ($X$, $Y = 3$, 4) ion pairs at the corner and step sites of MgO(001) are within 49−72 kcal/mol, while on an $O_{5C}$ terrace site the binding energy is only 25.3 kcal/mol. This indicates that the decomposition of $N_2O$ to $N_2$ and $O_{ad}$ is thermodynamically favorable at those defective sites considered but thermodynamically unfavorable at the terrace sites. This result is in agreement with the prediction of Nygren and Pettersson.[13]

In Table 4, we report the geometries of the transition states and the corresponding barrier heights for $N_2O$ decomposition at the terrace anion on the MgO(001) surface. These results are obtained by B3LYP and MP2 calculations with embedded $(MgO)_5$ and $(MgO)_9$ cluster models. The decomposition was modeled by supposing a linear $N_2O$ molecule impacting vertically onto a terrace $O_{5C}$ anion, according to that found in the previous studies regarding $N_2O$ decomposition on CaO.[11,12] On the basis of the data listed in Table 4, we may conclude the following. (i) Judging from the geometric data and the calculated barrier heights with $(MgO)_9$ and $(MgO)_5$ cluster models, the cluster size dependence is small but nonnegligible at both MP2 and B3LYP levels. However, the calculated reaction heats vary substantially from smaller to larger cluster models. (ii)The geometric data of the transition states and the reaction heats predicted by B3LYP differ to some extent from those by MP2. The B3LYP barrier heights are around 16 kcal/mol lower than those obtained by MP2, in line with the finding that the B3LYP would underestimate the barrier heights.[22] (iii) The MP2 and B3LYP barrier heights on the embedded $(MgO)_9$ cluster are 53 and 36 kal/mol, respectively. These are in good agreement with the previous MP2 value of 51 kcal/mol and with the CASPT2N value of 33 kcal/mol obtained by using an embedded $[Mg_5O]^{8+}$ cluster model.[17,39] The overall experimental activation energy was reported to be around 35 kcal/mol.[1,17] It would be possible for $N_2O$ to decompose over a five-coordinate $O^{2-}$ anion on MgO(001), while its endothermicity could be compensated by the exothermicity of the subsequent combination of O adatoms giving rise to $O_2$ desorption. Indeed, the calculated low binding energy of 25.3 kcal/mol for O adatoms on terrace anions on MgO implies that the step, i.e., $2O_a \rightarrow O_2$(g), is highly exothermic (about −70 kcal/mol).

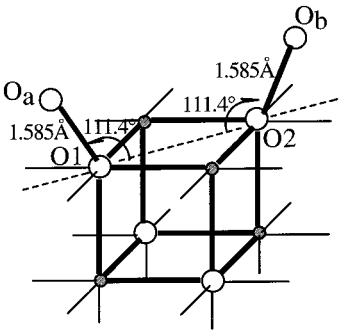


**Figure 4.** Cooperative adsorption of two O atoms on an $O_{5C}-O_{5C}$ anion pair on MgO(001) surface. The whole system has a $C_{2v}$ symmetry.

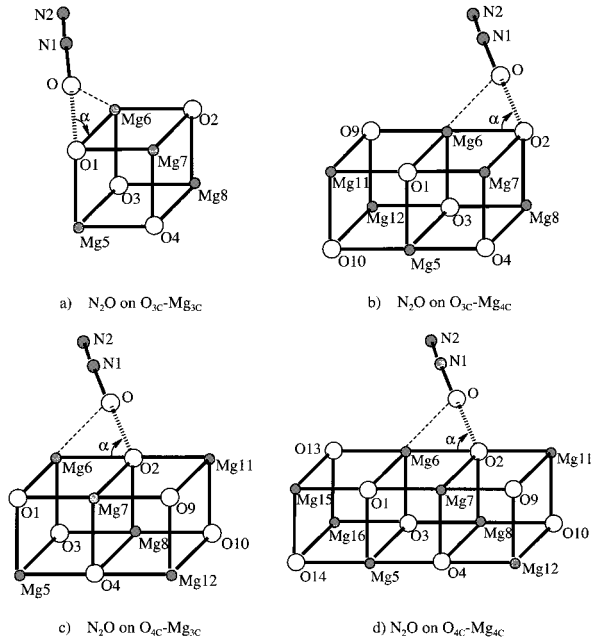


**Figure 5.** Geometries of transition states of $N_2O$ decomposition over (a) $O_{3C}-Mg_{3C}$, (b) $O_{3C}-Mg_{4C}$, (c) $O_{4C}-Mg_{3C}$, (d) $O_{4C}-Mg_{4C}$ pair sites modeled by the embedded $(MgO)_n$ clusters.

We have checked another possibility that two $N_2O$ molecules may cooperatively decompose on a pair of regular sites, namely, an $O_{5C}-O_{5C}$ pair site. The $O_{5C}-O_{5C}$ ion pair on the MgO(001) surface was modeled by a $(MgO)_4$ cluster embedded in a (10 × 10 × 10) microcrystal. The optimized geometry for this cooperative adsorption of two oxygen atoms is presented in Figure 4. The binding energy for this mode is found to be 57 kcal/mol, by far smaller than the energy cost of ~89 kcal/mol required to decompose simultaneously two $N_2O$ molecules, showing that cooperative decomposition of two $N_2O$ molecules on a pair of surface anions is unlikely.

**4. $N_2O$ Decomposition over Low-Coordinate Sites on MgO**. For the reaction of $N_2O$ decomposition on the $O_{XC}-Mg_{YC}$ ($X$, $Y = 3$, 4) pair sites, both reactants and products will

**TABLE 5: Transition States, Barrier Heights,[a] and Reaction Heats[b] for $N_2O$ Decomposition on MgO (B3LYP Calculations)**

| pair site | cluster model | | $R_{OMg}$ (Å) | $R_{OO}$ (Å) | $R_{NO}$ (Å) | $R_{NN}$ (Å) | α | $E^{TS}$ (kcal/mol) | $-\Delta E$ (kcal/mol) |
|---|---|---|---|---|---|---|---|---|---|
| $O_{3C}-Mg_{3C}$ | $(MgO)_4$ | island | 2.036 | 2.096 | 1.558 | 1.116 | 58.0 | 20.5 (24.8) | 28.0 (16.0) |
| $O_{3C}-Mg_{4C}$ | $(MgO)_6$ | corner (A) | 2.067 | 2.006 | 1.584 | 1.114 | 60.3 | 28.3 (30.3) | 9.4 (5.4) |
| $O_{4C}-Mg_{3C}$ | $(MgO)_6$ | corner (B) | 2.041 | 2.090 | 1.575 | 1.114 | 58.2 | 24.2 (25.5) | 13.9 (11.5) |
| $O_{4C}-Mg_{4C}$ | $(MgO)_8$ | step | 2.071 | 2.010 | 1.600 | 1.114 | 60.4 | 28.9 (31.8) | 5.4 (0.9) |

[a] $E^{TS} = [(MgO)_n-O-N_2] - E[(MgO)_n] - E(N_2O)$. [b] $\Delta E = E[(MgO)_n-O] + E(N_2) - E[(MgO)_n] - E(N_2O)$. [c] Values in parentheses are obtained by using bare cluster models.

be singlets. The transition states of $N_2O$ decomposition on the $O_{XC}-Mg_{YC}$ ($X, Y = 3, 4$) ion pairs have been determined and depicted in Figure 5. The corresponding geometry parameters, barrier heights, and the reaction heats are given in Table 5.

For all cases, the transition states possess a nearly linear arrangement of $N_2-O-O_{XC}$ configuration, in line with that found in the previous studies regarding $N_2O$ decomposition on CaO.[11,12] Snis and co-workers[11] suggested only single surface anions be involved in the activation of $N_2O$ on the CaO(001) terrace site or on a corner site and proposed the following decomposition mechanism, i.e., the $N_2$-to-O $\pi$-bond and $\sigma$-bonds are weakened and finally broken, while an $O-O^{2-}$ $\sigma$-bond is formed. This mechanism is generally supported by the present calculations except that, similar to what we have found for O atomic adsorption, we would like to emphasize the role of nearby cations. We found that the nearby low-coordinated $Mg_{YC}$ ($Y = 3, 4$) cations are also involved in the activation of the $N_2O$ molecule by stabilizing the transition state via a substantial dative interaction between the lone pair on the O atom of the $N_2O$ molecule and an empty orbital on the $Mg_{YC}$ site. NBO analysis performed on the SCF wave function of the transition state of $N_2O$ decomposition on the $Mg_{3C}-O_{4C}$ site of the $(MgO)_6$ cluster, for example, reveals two important charge-transfer interactions, i.e., the first one (interaction energy: ~48.4 kcal/mol) is between a lone pair at the active $O_{4C}$ sites and the O−N antibonding orbital of the $N_2O$ molecule, and the second one (interaction energy: ~17.2 kcal/mol) is between two lone pairs on the O atom of the $N_2O$ molecule and an empty orbital on the $Mg_{3C}$ site.

As shown in Table 5, the barrier heights calculated by using embedded cluster models vary from 20.5 kcal/mol on the most active $O_{3C}-Mg_{3C}$ pair site to 28.9 kcal/mol on the $O_{4C}-Mg_{4C}$ pair site. On the basis of the calculated barrier heights and reaction heats, the following order of activity toward $N_2O$ decomposition can be assigned: $O_{3C}-Mg_{3C} > O_{4C}-Mg_{3C} > O_{3C}-Mg_{4C} > O_{4C}-Mg_{4C}$. Note that the same trend can be predicted by using bare cluster models except that the bare cluster model tends to give higher barrier heights and lower reaction heats. Furthermore, it is worthy to note that the calculated barrier heights over the defect sites are considerably smaller than those over the terrace sites, indicating that $N_2O$ decomposition is more feasible over the low coordinate $O_{XC}-Mg_{YC}$ ($X, Y = 3, 4$) pair sites.

**5. $N_2O$ Decomposition on Li/MgO**. For the embedded $[Li^+O^-]$ center, both B3LYP and MP2 methods predicted that it has an $^2A$ ground state (local symmetry of $C_{4v}$) and a low-lying $^2E$ state. The predicted excitation energies are 11.2 and 13.0 kcal/mol by B3LYP and MP2 methods, respectively. At the $^2E$ state, the electron hole is well localized on the $p_\pi$ orbital of the anion. After atomic oxygen adsorption on top of the $O_{5C}^-$ anion of this $[Li^+O^-]$ center, the whole system has an $^2E$ ground state. By use of the B3LYP method, the calculated $O_{ad}-O_{5C}^-$ bond length is 1.365 Å, close to the experimental values of 1.34 and 1.33 Å reported for superoxy ions in the gas phase[40] and in solid $LiO_2$,[41] respectively. The calculated vibrational frequency

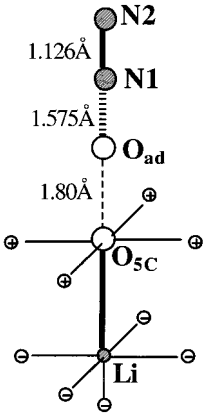


**Figure 6.** Geometry of the transition state of $N_2O$ decomposition on the $[Li^+O^-]$ center.

for the stretching mode of the $O_{ad}-O_{5C}^-$ bond is 1134 $cm^{-1}$, in line with those (1134−1164 $cm^{-1}$) of superoxy anions in crystalline alkali metal superoxides.[42,43] All this evidence as well as the detailed Mulliken population analysis demonstrated that the so-formed $[O_{ad}-O_{5C}]$ dioxygen species is of $O_2^-$ character. The calculated binding energy of atomic oxygen adsorption on the $O_{5C}^-$ anion is 71.4 kcal/mol. By use of the MP2 method, the optimal $O_{ad}-O_{5C}^-$ bond length is 1.34 Å and the binding energy is 59.3 kcal/mol. Therefore, both methods predicted that the decomposition of $N_2O$ on the $[Li^+O^-]$ center is exothermic. The increased activity toward $N_2O$ decomposition upon Li-doping in MgO could be attributed to the $[Li^+O^-]$ centers abundant on the surface. Experimentally, it was shown that Li-doping induces not only the existence of a number of $[Li^+O^-]$ centers on the catalyst[44] but also an increase of the number of high-index surface sites.[45]

In the linear arrangement of the transition state (cf. Figure 6) of $N_2O$ decomposition on the $[Li^+O^-]$ center, the intermolecular $O_{5C}^- - O_{ad}$ distance of 1.80 Å and the intramolecular $O_{ad}-N$ bond length of 1.57 Å are obtained by using the B3LYP method. The calculated activation energy for $N_2O$ decomposition over the $[Li^+O^-]$ center is 47.4 kcal/mol, in good agreement with the experimental value of 46 ± 2 kcal/mol determined by Lunsford et al.[7] Such an agreement is fortuitous when the results from MP2 calculations and larger cluster models (cf. Table 4) are considered.

When a larger, embedded $LiMg_4O_5$ cluster was used to simulate the $[Li^+O^-]$ center, the B3LYP method unfortunately failed to give a localized electron hole on the $[Li^+O^-]$ center. Spin density analysis based on the B3LYP-derived wave functions of the embedded $LiMg_4O_5$ cluster shows that the spin density on the central $O_{5C}$ atom is only ~0.5. This would be one of the reasons for the substantial discrepancy of ~12 kcal/mol found between the two B3LYP barrier heights derived from the embedded LiO dimer and the embedded $LiMg_4O_5$ cluster model.

It should be more meaningful to compare the calculated barrier heights on $(MgO)_5$ with those on $LiMg_4O_5$ (cf. Table

4). B3LYP predicts that Li-doping reduces the activation energy from 42.0 to 35.6 kcal/mol, while MP2 shows a 9.9 kcal/mol energy lowering of the transition state when a Mg is replaced by a Li. This demonstrates that the promotion effect of Li-doping to the $N_2O$ decomposition should be due to the existence of $[Li^+O^-]$. Moreover, note that the decomposition of $N_2O$ on the $[Li^+O^-]$ center leads to the formation of superoxide ion ($O_2^-$). This may account for the high $C_2$ selectivity of Li/MgO catalysts in OCM reaction,[8] i.e., the so-formed $O_2^-$ species might be the specific selective oxygen species for $C_2$ products.

## Concluding remarks

The main results of the present study regarding atomic oxygen adsorption and $N_2O$ decomposition on MgO and Li-doping MgO(001) surfaces can be summarized as follows.

(1) On the MgO(001) terrace, atomic oxygen is adsorbed on top of the $O_{5c}$ anions, while on corners or steps, the preferable mode is for atomic oxygen to bridge over the low-coordinated $O_{XC}-Mg_{YC}$ ($X$, $Y = 3$, 4) ion pairs. The adsorption of atomic oxygen leads to the formation of a peroxide ion. The calculated binding energies for the adsorption on a terrace site is around 20 kcal/mol, by far lower than those (49−72 kcal/mol) on the low-coordinated $O_{XC}-Mg_{YC}$ pair sites. The calculated $O_{ad}-O_{XC}$ stretching frequencies of peroxide ions formed at corners and steps are in the range 819−857 $cm^{-1}$. For the adsorption on the $O_{XC}-Mg_{YC}$ ($X$, $Y = 3$, 4) pair sites, NBO analysis demonstrates that apart from the $O_{ad}-O_{XC}$ bonding, there exists substantial charge transfer between the lone pair on an O adatom and the empty orbital on $Mg_{YC}$, which may favor the O-exchange between the O adatom and the lattice O anion.

(2) $N_2O$ decomposition over a five-coordinate terrace anion would be possible, and the defective $O_{XC}-Mg_{YC}$ ($X$, $Y = 3$, 4) ion pairs are more active for decomposing $N_2O$. The activity of the $O_{XC}-Mg_{YC}$ ($X$, $Y = 3$, 4) ion pairs toward $N_2O$ decomposition could be assigned in the order $O_{3C}-Mg_{3C} > O_{4C}-Mg_{3C} > O_{3C}-Mg_{4C} > O_{4C}-Mg_{4C}$.

(3) When the MgO catalyst is doped with Li, the so-called $[Li^+O^-]$ centers are found to be active for decomposing $N_2O$, which accounts for the promotion effect of Li-doping on the catalytic reaction. The decomposition of $N_2O$ on the active $[Li^+O^-]$ center leads to the formation of the superoxide anion, which would be the reason for the high $C_2$ selectivity in the OCM reaction.

**Acknowledgment.** This work is partially supported by the National Nature Science Foundation of China (NSFC), the doctoral project foundation of the Education Ministry of China, and Fok Ying Tung Education Foundation.

## References and Notes

(1) Winter, E. R. S. *J. Catal*. **1970**, *19*, 32.
(2) Ward, M. B.; Lin, M. J.; Lunsford, J. H. *J. Catal*. **1977**, *50*, 306.
(3) Ito, T.; Wang, J.-X.; Lin, C. H.; Lunsford, J. H. *J. Am. Chem. Soc*. **1985**, *107*, 5062.
(4) Iwasawa, Y.; Nakamura, T.; Takamatsu, K.; Ogasawara, S. *J. Chem. Soc., Faraday Trans. 1* **1980**, *76*, 939.
(5) Nakamura, M.; Mitsuhashi, H.; Takezawa, N. *J. Catal*. **1992**, *138*, 686.
(6) Nakamura, M.; Fujita, S.; Takezawa, N. *Catal. Lett.* **1992**, *14*, 315.
(7) Yamamoto, H.; Chu, H. Y.; Xu, M.; Shi, C.; Lunsford, J. H. *J. Catal*. **1993**, *142*, 325.
(8) Hutchings, G. J.; Scurrell, M. S.; Woodhouse, J. R. *Chem. Soc. Rev.* **1989**, *18*, 251.
(9) Kobayashi, H.; Kobayashi, M. *Catal. Rev. Sci. Eng*. **1974**, *10*, 139.
(10) Nakamura, M.; Yanagibishi, H.; Mitsuhashi, H.; Takezawa, N. *Bull. Chem. Soc. Jpn.* **1993**, *66*, 2467.
(11) Snis, A.; Stromberg, D.; Panas, I. *Surf. Sci*. **1993**, *292*, 317.
(12) Kantorovich, L. N.; Gillan, M. J. *Surf. Sci.* **1997**, *376*, 169.
(13) Nygren, M. A.; Pettersson, L. G. M. *Chem. Phys. Lett*. **1994**, *230*, 456.
(14) Kantorovich, L. N.; Gillan, M. J.; White, J. A. *J. Chem. Soc., Faraday Trans.* **1996**, *92*, 2075.
(15) Kantorovich, L. N.; Gillan, M. J. *Surf. Sci.* **1997**, *374*, 373.
(16) Herzberg, G. *Electronic spectra of polyatomic molecules*; Van Nostrand Reinhold: New York, 1966.
(17) Snis, A.; Miettinen, H. *J. Phys. Chem. B* **1998**, *102*, 2555.
(18) Ito, T.; Lunsford, J. H. *Nature* **1985**, *314*, 721.
(19) Børve, K. J.; Pettersson, L. G. M. *J. Phys. Chem*. **1991**, *95*, 7401.
(20) Anchell, L. J.; Morokuma, K.; Hess, A. C. *J. Chem. Phys.* **1991**, *99*, 6004.
(21) Johnson, M. A.; Stefanovich, E. V.; Truong, T. N. *J. Phys. Chem. B* **1997**, *101*, 3196.
(22) Ackermann, L.; Gale, J. D.; Catlow, C. R. A. *J. Phys. Chem. B* **1997**, *101*, 10028.
(23) Benzon, S. W. In *Organic Peroxides*; Shaw, A., Ed.; Wiley Interscience: New York, 1970; Vol. 1, Chapter 2.
(24) Wyckoff, R. W. G. *Crystal Structures*; Wiley: New York, 1963.
(25) Xu, X.; Nakatsuji, H.; Ehara, M.; Lu, X.; Wang, N.; Zhang, Q. *Sci. China B* (in English) **1998**, *41*, 113.
(26) Xu, X.; Lu, X.; Wang, N.; Zhang, Q. *Chem. Phys. Lett.* **1995**, *235*, 541.
(27) Lu, X.; Xu, X.; Wang, N.; Zhang, Q.; Nakatsuji, H.; Ehara, M. *J. Phys. Chem. B*, submitted.
(28) Birkenheuer, U.; Boettger, J. C.; Rösch, N. *J. Chem. Phys*. **1994**, *100*, 6826.
(29) Stevens, W. J.; Basch, H.; Krauss, M. *J. Chem. Phys.* **1984**, *81*, 6026.
(30) Becke, A. D. *J. Chem. Phys*. **1993**, *98*, 5648.
(31) Lee, C.; Yang, W.; Parr, R. G. *Phys. Rev. B* **1988**, *37*, 785.
(32) Frisch, M. J.; Trucks, G. W.; Schlegel, H. B.; Gill, P. M. W.; Johnson, B. G.; Robb, M. A.; Cheeseman, J. R.; Keith, T.; Petersson, G. A.; Montgomery, J. A.; Raghavachari, K.; Al-Laham, M. A.; Zakrzewski, V. G.; Ortiz, J. V.; Foresman, J. B.; Peng, C. Y.; Ayala, P. Y.; Chen, W.; Wong, M. W.; Andres, J. L.; Replogle, E. S.; Gomperts, R.; Martin, R. L.; Fox, D. J.; Binkley, J. S.; Defrees, D. J.; Baker, J.; Stewart, J. P.; Head-Gordon, M.; Gonzalez, C.; Pople, J. A. *Gaussian 94*; Gaussian, Inc.: Pittsburgh, PA, 1995.
(33) Foster, J. P.; Weinhold, F. *J. Am. Chem. Soc.* **1980**, *102*, 7211. Reed, A. E.; Curtiss, L. A.; Weinhold, F. *Chem. Rev.* **1988**, *88*, 899.
(34) Møller, C.; Plesset, M. S. *Phys. Rev.* **1934**, *46*, 618.
(35) Head-Cordon, M.; Pople, J. A.; Frisch, M. J. *Chem. Phys. Lett*. **1988**, *153*, 503.
(36) Che, M.; Tench, A. J. In *Advance in Catalysis*; Eley, D. D., Pines, H., Weisz, P. B., Eds.; Academic Press: New York, 1983; Vol. 32, p 8 and references therein.
(37) Jones, R. D.; Summerville, D. A.; Basolo, F. *Chem. Rev.* **1979**, *79*, 139.
(38) Lunsford, J. H.; Yang, X.; Haller, K.; Laane, J.; Mestl, G.; Knözinger, H. *J. Phys. Chem.* **1993**, *97*, 13810.
(39) Snis, A.; Miettinen, H. Unpublished results, private communication.
(40) Celotta, R. J.; Bennett, A.; Hall, J. L.; Siegel, M. W.; Levine, J. *Phys. Rev. A* **1972**, *6*, 631.
(41) Vaska, L. *Acc. Chem. Res.* **1976**, *9*, 175.
(42) Blunt, F. J.; Hendra, P. J.; Mackenzie, J. R. *Chem. Commun*. **1969**, 278.
(43) Bates, J. B.; Brooker, M. H.; Boyd, G. E. *Chem. Phys. Lett*. **1972**, *16*, 391.
(44) Wang, J.-X.; Lunsford, J. H. *J. Phys. Chem.* **1986**, *90*, 5883.
(45) Hargreaves, J. S. J.; Hutchings, G. J.; Joyner, R. W.; Kiely, C. J. *J. Catal.* **1992**, *135*, 576.